Highly selective production of gasoline-range hydrocarbons via hydroconversion of polyolefins over Ru/CeO2 and BEA hybrid catalysts

Junho Suh[a], Hyeongdong Jung[a], Joonkeol Yoon[a], Jae-Soon Choi[b], Jungup Bang[b], Do Heui Kim[a,*]

[a]*School of Chemical and Biological Engineering, Institute of Chemical Processes, Seoul National University, 1 Gwanak-ro, Gwanak-Gu, Seoul 08826, the Republic of Korea*

[b]*Catalyst R&D, LG Chem., 188 Munji-ro, Yuseong-gu, Daejeon 34122, the Republic of Korea*

[*]Corresponding author: dohkim@snu.ac.kr

Text S1. Catalyst preparation

CeO_2 was obtained from Rhodia and calcined in a static muffle furnace at 550°C for 5 h (ramping rate = 5°C/min). 5 wt% of Ru was impregnated on CeO_2 using incipient wetness impregnation method. Calculated amount of ruthenium (III) chloride hydrate ($RuCl_3 \cdot xH_2O$, 99.9% (PGM basis), Ru 38% min, Alfa Aesar) was dissolved in ultrapure water to make a Ru precursor solution and the solution was added dropwise to the CeO_2. The impregnated catalyst was dried overnight at 105°C in a convection oven and then reduced in a flow reactor at 400°C for 3 h (ramping rate = 5°C/min) under 100 mL/min flowing gas of 10% H_2/N_2. For the ease of catalyst handling and storage, the reduced catalyst was passivated under the flow of 5% O_2/N_2.

The as-synthesized Ru/CeO_2 catalyst was mixed with various zeolites and solid acids to obtain hybrid catalysts. Beta zeolite (BEA structure, Si/Al_2 = 25, 38, and 360, Alfa Aesar), Y zeolite (FAU structure, Si/Al_2 = 30, Alfa Aesar), ZSM-5 zeolite (MFI structure, Si/Al_2 = 23, Alfa Aesar), ferriorite zeolite (FER structure, Si/Al_2 = 20, Alfa Aesar), SSZ-13 zeolite (CHA structure, Si/Al_2 = 23, Heesung Catalysts) and mordenite zeolite (MOR structure, Si/Al_2 = 20, Alfa Aesar) were calcined at 550°C for 5 h in a muffle furnace under static air before mixing (ramping rate = 5°C/min). Al_2O_3 was prepared by the calcination of Boehmite (Sasol) at 500°C for 4 h in a static muffle furnace (ramping rate = 5°C/min). WO_3-TiO_2 (W:Ti = 1:9 in a molar ratio) was synthesized by hydrolyzing titanium isopropoxide ($Ti(OCH(CH_3)_2)_4$, 99.999% trace metals basis, Sigma Aldrich) with tungsten precursor solution which was made with ammonium metatungstate hydrate ($(NH_4)_6H_2W_{12}O_{40} \cdot xH_2O$, 99.99% trace metals basis, Sigma-Aldrich) for 24 h, followed by filtration, drying overnight in a 105°C oven, and calcination at 500°C for 4 h in a muffle furnace (ramping rate = 2°C/min). SiO_2-Al_2O_3 (Sigma Alrdich) was calcined at 550°C for 5 h in a muffle furnace (ramping rate = 5°C/min). Ru/CeO_2 and a variety

of zeolites and solid acids were mixed by grinding for more than 10 minutes in a mortar. The mixing ratio of X:Y (Ru/CeO_2:zeolite or solid acid = X:Y) in the catalyst was based on a mass ratio.

Ru/BEA was prepared via wet impregnation method. 5 wt% of Ru was impregnated on BEA using ruthenium (III) chloride hydrate ($RuCl_3 \cdot xH_2O$, 99.9% (PGM basis), Ru 38% min, Alfa Aesar). Ru precursor and BEA were put together in ultrapure water under vigorous stirring and the solvent was evaporated using rotary evaporator. Then the impregnated catalyst was dried overnight at 105°C in a convection oven and reduced in a flow reactor at 400°C for 3 h (ramping rate = 5°C/min) under 100 mL/min flowing gas of 10% H_2/N_2. For the ease of catalyst handling and storage, the reduced catalyst was passivated under the flow of 5% O_2/N_2.

Text S2. Characterization methods

The absorption spectra of the liquid products obtained from the hydroconversion of LDPE were measured on a UV-VIS spectrophotometer (JASCO V-770 UV-visible/NIR spectrophotometer) in the wavelength range of 190-800 nm using a quartz cuvette with path length of 1 cm. n-Octane was used as a reference and the liquid samples were diluted with octane to identify the absorption peaks under the detection limit.

Textural properties of the catalysts were measured from N_2 adsorption-desorption experiments using a BELSORP-mini II instrument (BEL Japan). In advance of the analysis, 0.05-0.1 g of the catalysts were degassed at 200°C for 3 h to eliminate adsorbed impurities. Specific surface area was calculated by Brunauer-Emmett-Teller (BET) equation and pore volume and average pore diameter were analyzed by Barrett-Joyner-Halenda (BJH) method.

Ammonia-temperature programmed desorption (NH_3-TPD) was carried out in BEL-CAT-II apparatus (BEL Japan) to measure the acidic property of the catalysts. About 0.05 g of each catalyst was heated at 300°C for 1 h in order to remove physisorbed species and cooled to

50°C, followed by the saturation with 5% NH_3/He flow for 30 min and purging with pure He flow for 1 h to remove weakly adsorbed NH_3. Then, NH_3 desorption from the pretreated catalysts were monitored using a TCD through the temperature rise to 700°C at a ramping rate of 10°C/min under the pure He flow.

Pyridine-IR was performed using Nicolet 6700 Fourier-transform infrared spectrometer equipped with Praying Mantis diffuse reflectance accessory and mercury-cadmium-telluride detector. All samples were pretreated with 5% O_2/N_2 gas flow (50 mL/min) at 300°C for 30 min. Then the sample was cooled to 250°C and pyridine vapor was introduced until saturation. Physisorbed molecules were removed by purging under 50 mL/min nitrogen flow for 1 h and IR spectrum was recorded at 250°C. Peak at 1454 cm^{-1} represents Lewis acid sites and peak at 1542 cm^{-1} is related to Brønsted acid sites.[1, 2]

Metal dispersion and particle size of the Ru catalysts were estimated by pulse CO chemisorption using BEL-CAT-II (BEL Japan). The dispersion of Ru in Ru/CeO_2 was evaluated by cryo pulse CO chemisorption at -78°C to exclude the amount of CO adsorbed on CeO_2. 0.05 g of the catalysts were in situ pretreated with 5% H_2/Ar flow at 400°C for 30 min, followed by purging under He for 30 min. After cooling to -78°C using liquid nitrogen, a pulse of 4.98% CO/He was introduced until the sample was completely saturated, with a stoichiometric factor of CO/Ru = 1.

H_2-Temperature programmed reduction (H_2-TPR) curves were collected with BEL-CAT II apparatus (BEL Japan). Approximately 0.05-0.1 g of the samples were pretreated at 300°C for 1 h in Ar flow and cooled to 50°C. Then the temperature was raised to 950°C at the ramping rate of 10°C/min under a flow of 5% H_2/Ar, and the hydrogen consumption was detected using a TCD.

Powder X-ray diffraction (XRD) pattern of the catalysts was obtained in the range of 2θ = 5°-

80° with a Mode 1 Smartlab diffractometer (SmartLab, Rigaku) under 40 kV and 30 mA with Cu Kα radiation (0.154 nm).

Cs-corrected high resolution transmission electron microscopy (HRTEM) was performed using JEM-ARM200F microscope (JEOL Ltd.) equipped with spherical aberration corrector and cold field emission gun operating at an accelerating voltage of 200kV.

X-ray photoelectron spectroscopy (XPS) were conducted using VersaProbe K-alpha system (Ulvac-PHI, Japan) equipped with monochromatic Al Kα radiation source (1486.6 eV) to analyze the electronic state of Ru species on the catalyst surface. All the catalysts were pretreated under the ex-situ reduction at 400°C.

Thermogravimetric analysis (TGA) was conducted to detect the relative amount of coke deposited in the post-reaction catalysts using TG analyzer (TGA N-1000, Scinco).

Text S3. Activity test

Catalytic activity of polymer degradation was measured in a 25 mL Parr 5500 series reactor equipped with a mechanical stirrer attached to the top of the reactor and a Parr 4848 reactor control system. 3.5 g of low-density polyethylene (LDPE, M_n ~ 1,700, M_w ~ 4,000, cat. No 427772, Sigma Aldrich) and a certain amount of catalyst based on LDPE/catalyst ratio was loaded into the reactor. The reactor was then pressurized to 50 bar with H_2 to check out the possible leak of gaseous species, and purged with 25 bar of H_2 three times, followed by pressurizing to the reaction pressure. After measuring the mass of reactor, the reactor was heated to the reaction temperature (230-260°C) in about 40 minutes and the reaction was conducted for 4-16 h with 600 RPM of stirring rate. As soon as the reaction ended, the reactor was quickly moved to an ice bath to cool to under 20°C. Gas products and unreacted H_2 were collected in a gas cylinder and analyzed by an online gas chromatograph (6890N/G1530N,

Agilent Technologies) equipped with HP Plot-Q capillary column aligned with flame ionization detector (FID) and Carboxen-1000 packed column aligned with thermal conductivity detector (TCD). Prior to the collection of gas products, gas cylinder was flushed with air gun and vacuum state was created by using vacuum pump. Composition of the gas products were determined by using calibration gas mixture. After analyzing the gas products, remaining gas was vented and the mass of liquid and solid remainder in the reactor was measured. 20 mL of toluene (HPLC grade, 99.9%, Sigma Aldrich) was used to extract liquid products and solid residues. 20 μL of mesitylene (98%, Sigma Aldrich) was added as internal standard and liquid products were analyzed via gas chromatograph (Agilent 6890) equipped with a DB-5MS column aligned with FID. Response factors of each product in the liquid were calculated by using the alkane standard solution C_8-C_{20} and C_{21}-C_{40} (Supelco). Solid residues and post-reaction catalysts were filtered with toluene (anhydrous, 99.8%, Alfa Aesar) and acetone (97%, Samchun) and dried overnight at room temperature. Conversion, yield, selectivity, and isomer fraction in the products were calculated based on the following equations:

$$Conversion\ (\%) = \left(1 - \frac{Amount\ of\ unreacted\ reactant\ (g)}{Amount\ of\ initial\ reactant\ (g)}\right) \times 100\%$$

$$Yield\ (\%) = \left(\frac{Amount\ of\ C_i\ products\ (g)}{Amount\ of\ initial\ reactant\ (g)}\right) \times 100\%$$

$$Selectivity\ (\%) = \left(\frac{Amount\ of\ C_i\ products\ (g)}{Amount\ of\ total\ products\ (g)}\right) \times 100\%$$

$$Isomer\ fraction\ (\%) = \left(\frac{Amount\ of\ branched\ products\ (g)}{Amount\ of\ gas\ and\ liquid\ products\ (g)}\right) \times 100\%$$

In all hydroconversion reactions, carbon balances were in the range of 85-95% and missing part of the material balance was mainly due to the high volatility of the target gasoline products.

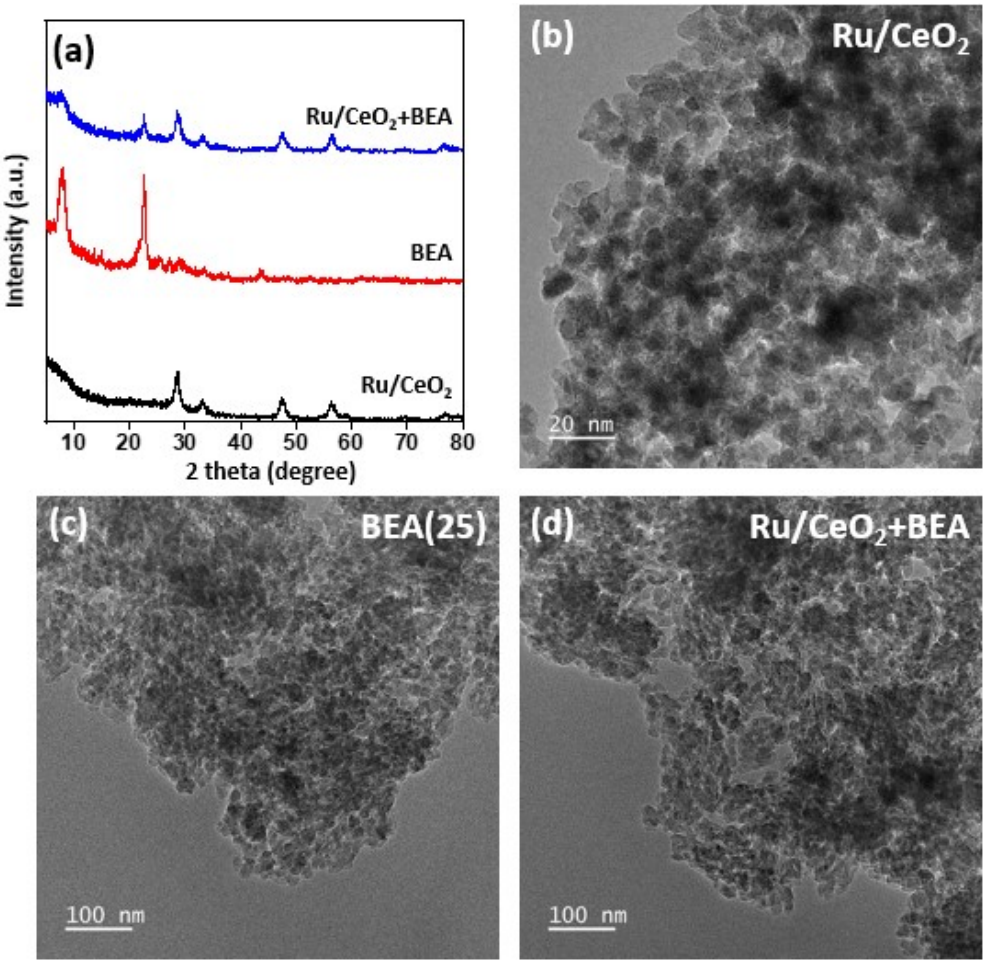

Fig. S1. (a) Powder X-ray diffraction and (b-d) HRTEM image of Ru/CeO_2, BEA(25) and Ru/CeO_2+BEA(mass ratio of Ru/CeO_2 to BEA = 1:2).

Table S1. Physicochemical properties of Ru/CeO_2, BEA(25), and Ru/CeO_2+BEA (mass ratio of Ru/CeO_2 to BEA = 1:2).

	BET Surface area $(m^2/g)^a$	**Pore diameter** $(nm)^b$	**Pore volume** $(cm^3/g)^c$
Ru/CeO_2	**128**	**7.7**	**0.25**
BEA(25)	**642**	**7.2**	**1.16**
Ru/CeO_2+BEA	**392**	**7.4**	**0.80**

[a]Calculated by the BET equation.

[b]Average pore diameter.

[c]Total pore volume at $P/P_0 = 0.99$.

Table S2. LDPE hydroconversion results over Ru/CeO_2, BEA(25), and Ru/CeO_2+BEA(25) catalysts. Reaction condition: 3.5 g LDPE, 0.25 g catalysts, 260°C, 50 bar H_2, 4 h

	LDPE conversion (%)	Gas product selectivity (%) (C_1-C_3)	Liquid product selectivity (%) (C_4 - C_{12})	(C_{13} - C_{20})	(C_{21} - C_{36})	Solid residue (%)	H_2 conversion (%)	Isomer fraction (%)	Carbon balance (%)
Ru /CeO_2	**99.9**	**15.7**	**38.0**	**32.6**	**13.6**	**0.1**	**74.3**	**21.1**	**84.9**
3:1	**100**	**9.7**	**49.4**	**32.2**	**8.6**	**0**	**58.0**	**41.0**	**92.8**
1:1	**99.3**	**1.5**	**96.4**	**1.4**	**0**	**0.8**	**42.7**	**81.0**	**92.7**
1:2	**98.8**	**1.5**	**95.4**	**1.6**	**0**	**1.2**	**40.3**	**79.9**	**95.1**
1:5	**98.8**	**1.2**	**97.0**	**0.4**	**0**	**1.4**	**48.5**	**80.0**	**87.6**
1:7	**98.7**	**1.1**	**97.1**	**0.3**	**0**	**1.5**	**46.9**	**79.7**	**86.5**
1:15	**98.5**	**0.7**	**96.3**	**1.1**	**0**	**1.8**	**40.4**	**80.9**	**85.7**
1:20	**96.0**	**0.7**	**93.7**	**1.2**	**0**	**4.5**	**30.9**	**81.5**	**90.9**
BEA (25)	**57.3**	**0.1**	**40.2**	**9.8**	**1.9**	**47.9**	**2.4**	**88.0**	**89.3**

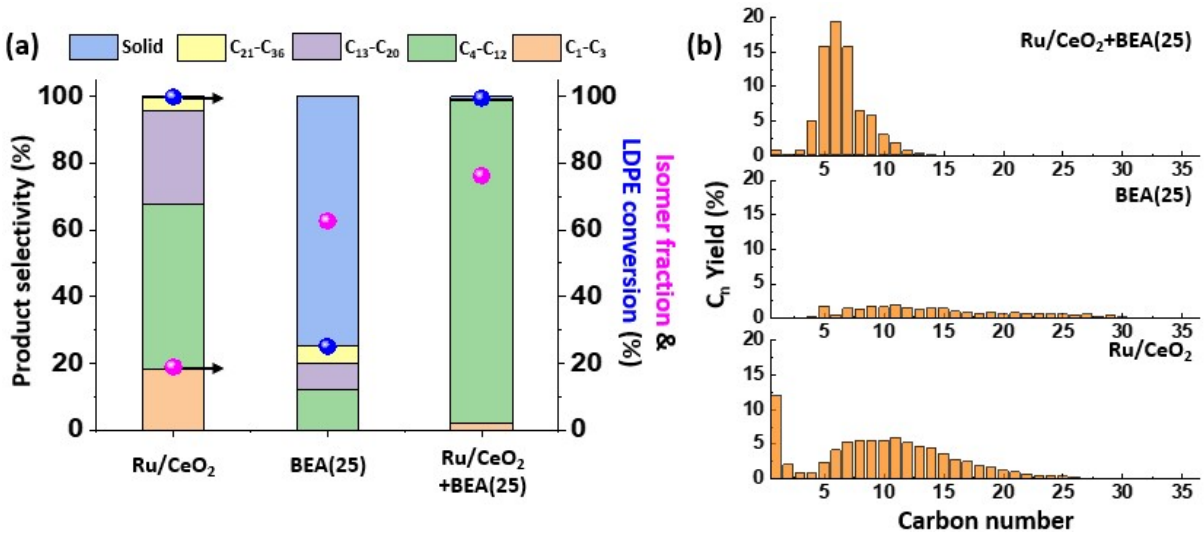

Fig. S2. (a) Product selectivity, LDPE conversion and isomer fraction in the gas and liquid products, and (b) product distribution over Ru/CeO_2, BEA(25), and Ru/CeO_2+BEA(25) catalysts (mass ratio of Ru/CeO_2 to BEA(25) = 1:2). Reaction condition: 3.5 g LDPE, 0.125 g catalysts, 250°C, 50 bar H_2, 16 h.

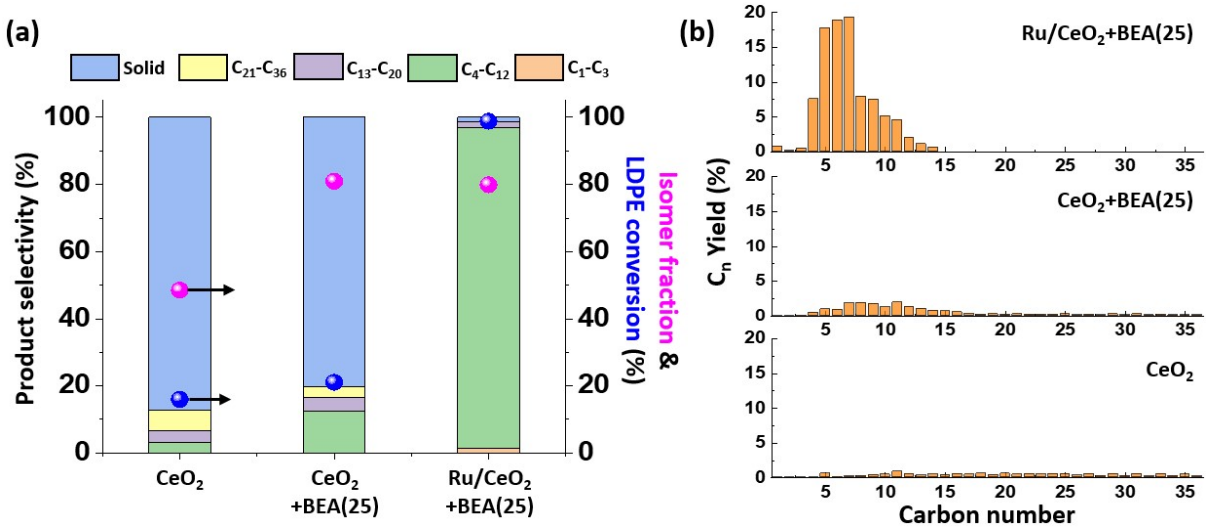

Fig. S3. (a) Product selectivity, LDPE conversion and isomer fraction in the gas and liquid products, and (b) product distribution over CeO_2, CeO_2+BEA(25), and Ru/CeO_2+BEA(25) catalysts (mass ratio of CeO_2 or Ru/CeO_2 to BEA(25) = 1:2). Reaction condition: 3.5 g LDPE, 0.25 g catalysts, 260°C, 50 bar H_2, 4 h.

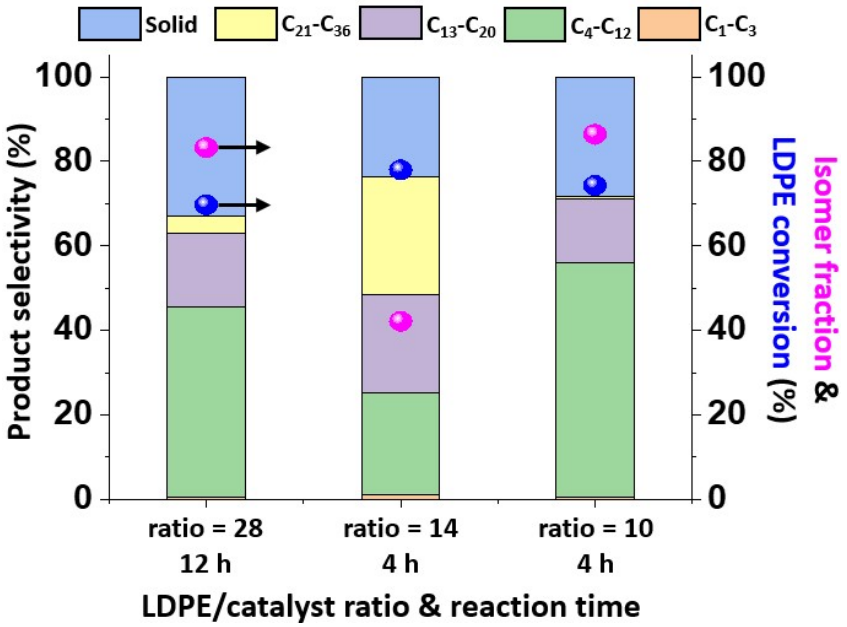

Fig. S4. (a) Product selectivity, LDPE conversion and isomer fraction in the gas and liquid products over different LDPE to catalyst ratio and reaction time. Reaction condition: 3.5 g LDPE, 50 bar H_2, mixing ratio of the Ru/CeO_2 to BEA = 1:2, 0.125g for LDPE/catalyst = 28 and 12 h, 0.25g for LDPE/catalyst = 14 and 4 h, 0.35g for LDPE/catalyst = 10 and 4 h.

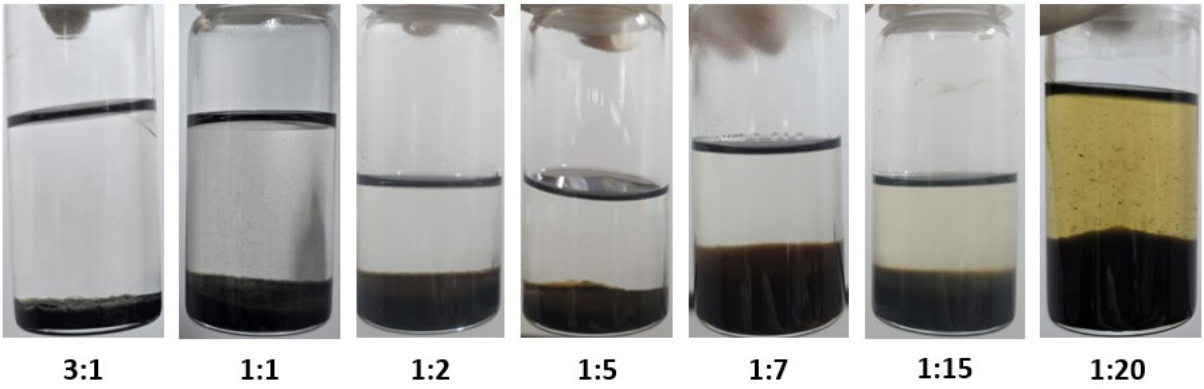

Fig. S5. Liquid products of LDPE hydroconversion, extracted with toluene, at different mass ratio of Ru/CeO_2 to BEA(25). Reaction condition: 3.5 g LDPE, 0.25 g catalysts, 260 °C, 50 bar H_2, 4 h

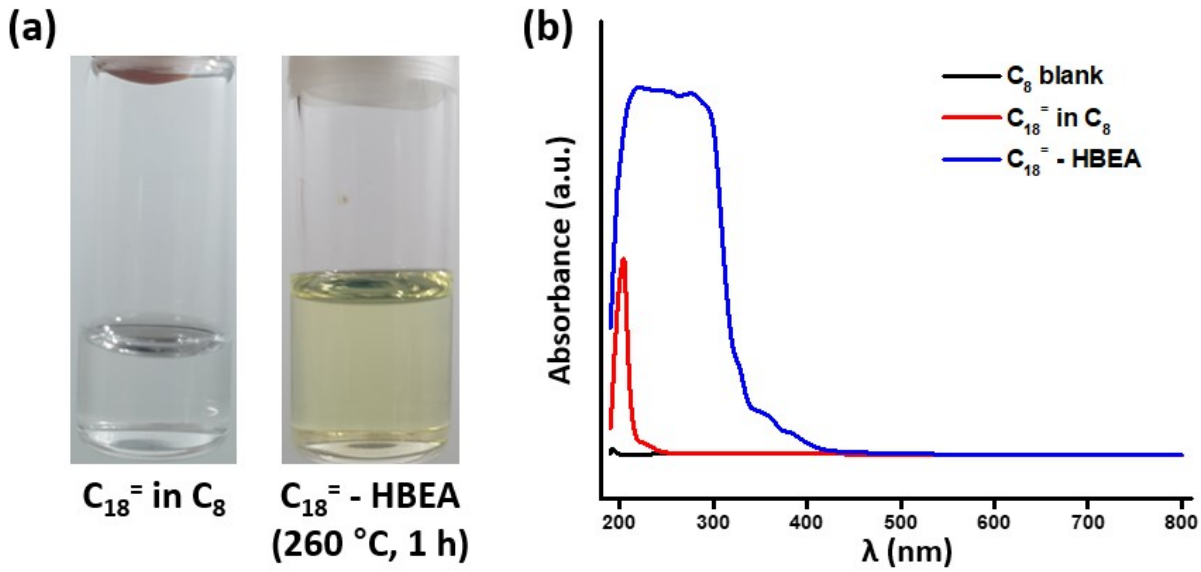

Fig. S6. (a) Octadecene($C_{18}^{=}$) in octane(C_8) solution and liquid products from $C_{18}^{=}$ hydrocracking under BEA catalyst. (b) UV-vis spectrum of C_8, $C_{18}^{=}$ in C_8 solution, and liquid products from $C_{18}^{=}$ hydrocracking under BEA. Reaction condition: Reaction condition: 3.5 g $C_{18}^{=}$, 0.25 g BEA(25), 260 °C, 50 bar H_2, 1 h

Table S3. Catalytic hydroconversion performance over various Ru-based catalysts.

Catalyst	Reaction conditions	Metal loading (%)	Yield of C_5-C_{12} or liquid (%)	Productivity ($g_{C5\text{-}C12}/g_{Ru}$·h or g_{liquid}/g_{Ru}·h)	Reference
Ru/CeO_2 +BEA (1:2)	270°C, 50 bar H_2, 2 h, PE/catalyst=14	0.5	(C_5-C_{12}) 82	3451	Thiw work
Ru/Al_2O_3 +BEA (1:1)	250°C, 30 bar H_2, 6 h, PE/catalyst=10	3	(C_5-C_{12}) 73	82	[3]
Ru/CeO_2	260°C, 30 bar H_2, 18 h, PP/catalyst=2.5	0.125	(liquid) 67	74	[4]
Ru/ZrO_2	240°C, 60 bar H_2, 4 h, PE/catalyst=34	5	(liquid) 84	25	[5]
Ru/BEA	215°C, 30 bar H_2, 16 h, PP/catalyst=14	5	(liquid) 69	12	[6]
Ru/FAU	200°C, 30 bar H_2, 16 h, PE/catalyst=14	5	(liquid) 67	12	[6]
Ru/TiO_2	250°C, 30 bar H_2, 16 h, PP/catalyst=20	5.9	(liquid) 66	14	[7]
Ru/CeO_2	240°C, 60 bar H_2, 8 h, PE/catalyst=34	5	(liquid) 90	77	[8]
Ru/ZSM-5	275°C, 45 bar H_2, 2 h, C_{16}/catalyst=2	2.5	(C_5-C_{16}) 7	3	[9]
Ru/WZr	250°C, 50 bar H_2, 2 h, PE/catalyst=40	5	(C_5-C_{12}) 19	77	[10]
Ru/TiO_2	225°C, 20 bar H_2, 4 h, PE/catalyst=20	5	(liquid) 71	71	[11]
Ru/SBA	230°C, 20 bar H_2, 5 h, PE/catalyst=75	3	(C_5-C_{12}) 23	113	[12]
Ru_1-ZrO_2	250°C, 15 bar H_2, 8 h, PE/catalyst=10	1.28	(liquid) 69	67	[13]

Table S4. Catalytic hydrocracking performance of various Pt, Rh and Ir-based catalysts.

Catalyst	Reaction conditions	Metal loading (%)	Yield of C_5-C_{12} (%)	Productivity (g_{C5-C12}/g_{metal}·h)	Productivity based on the metal price[a] ($g_{C5-C12}/\$_{metal}$·h)	Reference
Ru/CeO_2 +BEA (1:2)	270°C, 50 bar H_2, 2 h, PE/catalyst=14	0.5	82	3451	71	Thiw work
$Pt/WO_3/ZrO_2$	250°C, 30 bar H_2, 2 h, PE/catalyst=10	0.5	18	180	3	[14]
$Pt/WO_3/ZrO_2$ +BEA (1:1)	250°C, 30 bar H_2, 2 h, PE/catalyst=10	0.5	57	1140	16	[14]
$Pt/WO_3/ZrO_2$ +Y (1:1)	250°C, 30 bar H_2, 2 h, PE/catalyst=10	0.5	73	1460	21	[14]
Pt/BEA	315°C, 20 bar H_2, 1 h, PE/catalyst=10	1	30	300	4	[15]
$mSiO_2/Pt/SiO_2$	300°C, 8.9 bar H_2, 15 h, PE/catalyst=12	0.085	74	701	10	[16]
Pt/W/beta	250°C, 30 bar H_2, 1 h, PE/catalyst=40	2	64	1272	18	[17]
Pt-Ce/HY	300°C, 30 bar H_2, 2 h, PE/catalyst=10	5	81	81	1	[18]
Pt@S-1+BEA	250°C, 30 bar H_2, 2 h, PE/catalyst=10	0.3	89.5	2983	42	[19]
Rh/Nb_2O_5	300°C, 30 bar H_2, 6 h, PE/catalyst=10	3	47	26	0.1	[20]
Ir/HBEA	250°C, 30 bar H_2, 4 h, PE/catalyst=40	0.5	80	1604	10	[21]

[a] Price of each metals were Ru = 48.68 \$/g, Pt = 70.69 \$/g, Rh = 316.42 \$/g, and Ir = 163.42 \$/g at Jan 1, 2026, as reported by STRATEGIC METALS INVEST.

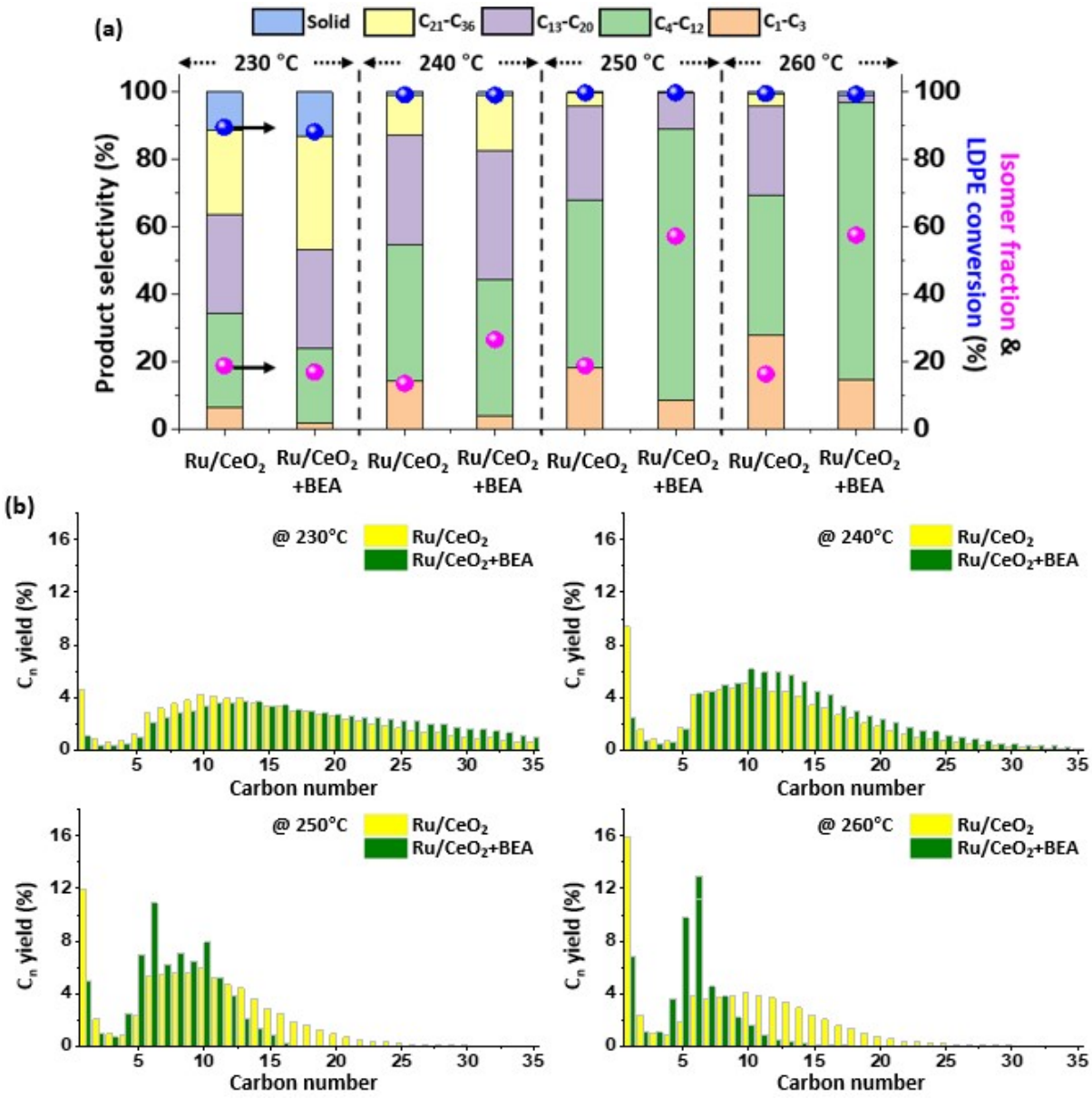

Fig. S7. (a) Product selectivity, LDPE conversion and isomer fraction in the gas and liquid products, and (b) product distribution at 230-260°C. Reaction condition: 3.5 g LDPE, 0.125 g catalysts, 50 bar H_2, 16 h, mixing ratio of the Ru/CeO_2 to BEA = 1:1.

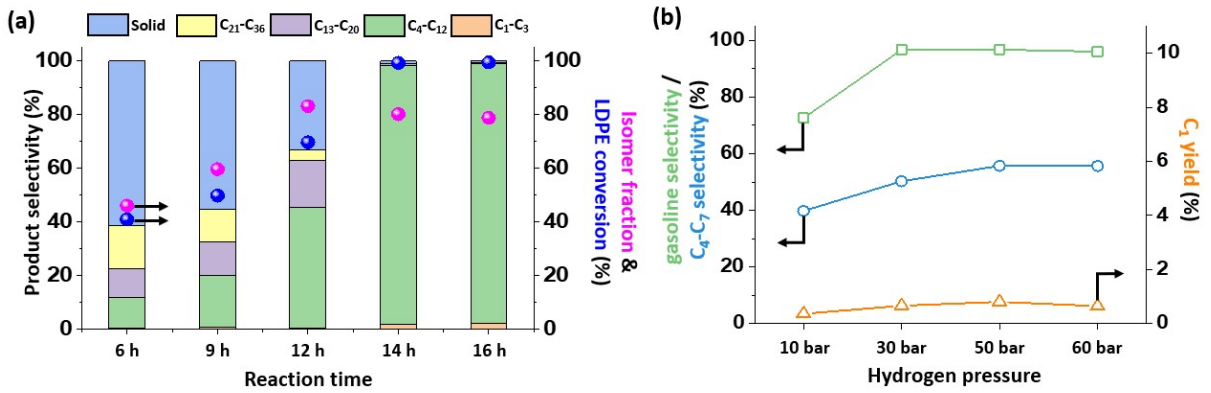

Fig. S8. (a) Product selectivity, LDPE conversion and isomer fraction in the gas and liquid products according to the reaction time, and (b) effect of initial hydrogen pressure on the Ru/CeO_2+BEA catalyst. Reaction condition: 3.5 g LDPE, 0.125 g catalysts, 250°C, (a) 6-16 h, 50 bar H_2, (b) 16 h, 10-60 bar H_2, mixing ratio of the Ru/CeO_2 to BEA = 1:2.

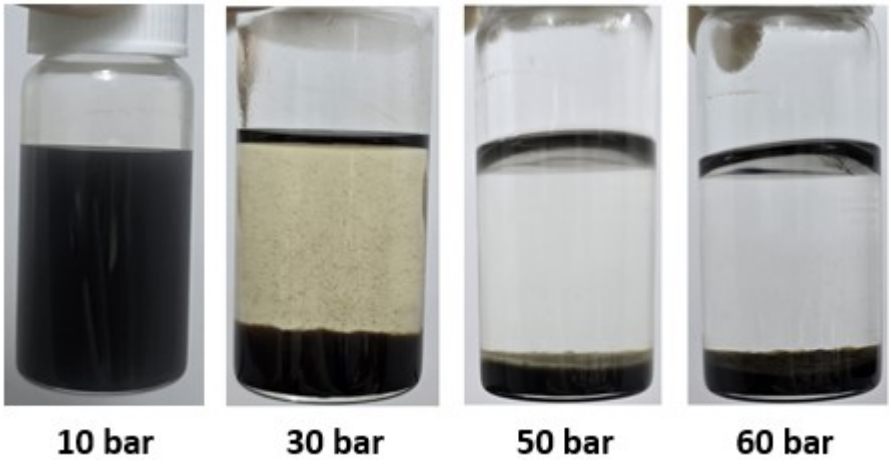

Fig. S9. Liquid products of LDPE hydroconversion at different hydrogen pressure. Reaction condition: 3.5 g LDPE, 0.125 g catalysts, 250 °C, 10-60 bar H_2, 16 h, mixing ratio of the Ru/CeO_2 to BEA = 1:2.

	BET surface area (m^2/g)[a]	Pore diameter (nm)[b]	Pore volume (cm^3/g)[c]	Total acidity (mmol/g)[d]	BAS/LAS ratio[e]
BEA(25)	**642**	**7.2**	**1.16**	**0.314**	**0.73**
Y(30)	**934**	**7.4**	**0.59**	**0.163**	**0.61**
ZSM-5(23)	**442**	**5.4**	**0.26**	**0.336**	**2.23**
FER(20)	**416**	**4.3**	**0.28**	**0.389**	**-**
SSZ-13(23)	**843**	**3.8**	**0.37**	**0.305**	**-**
MOR(20)	**575**	**6.5**	**0.36**	**0.400**	**-**
SiO_2-Al_2O_3	**508**	**4.2**	**0.53**	**0.501**	**-**

Table S5. Physicochemical properties of various zeolites.

[a]Calculated by the BET equation.

[b]Average pore diameter.

[c]Total pore volume at $P/P_0 = 0.99$.

[d]Measured by NH_3-TPD.

[e]Measured by pyridine-IR.

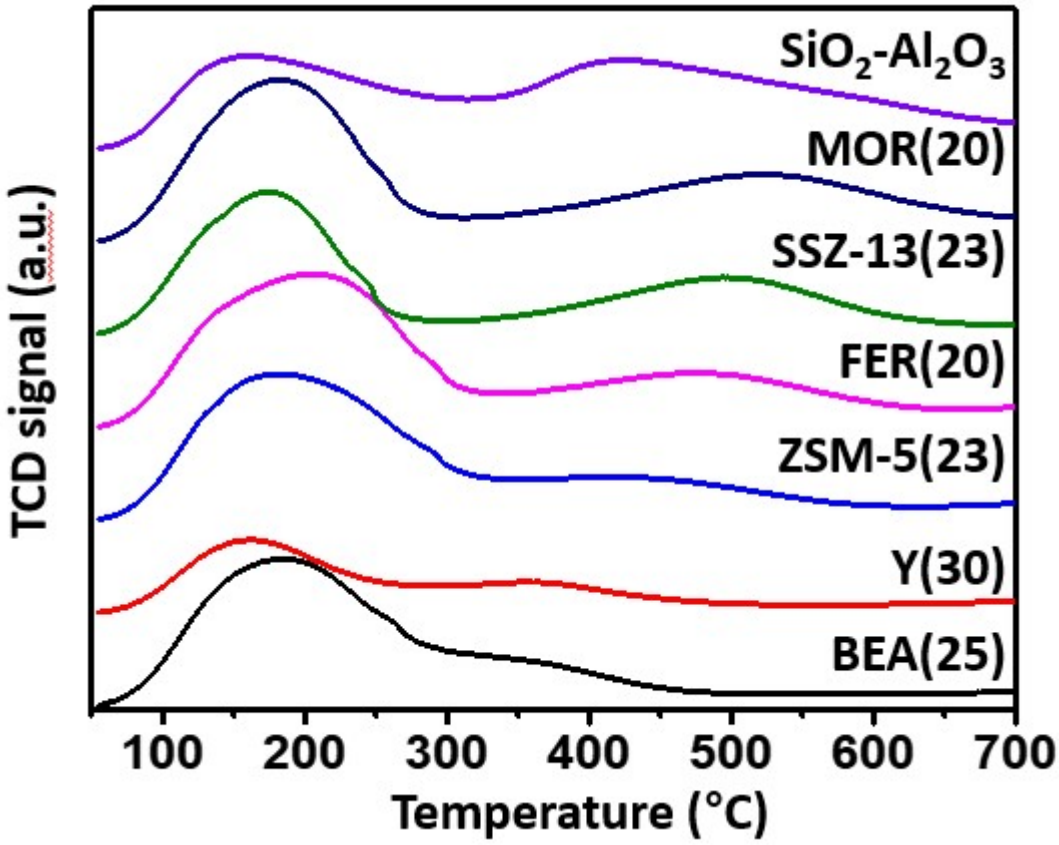

Fig. S10. NH_3-TPD of various zeolites.

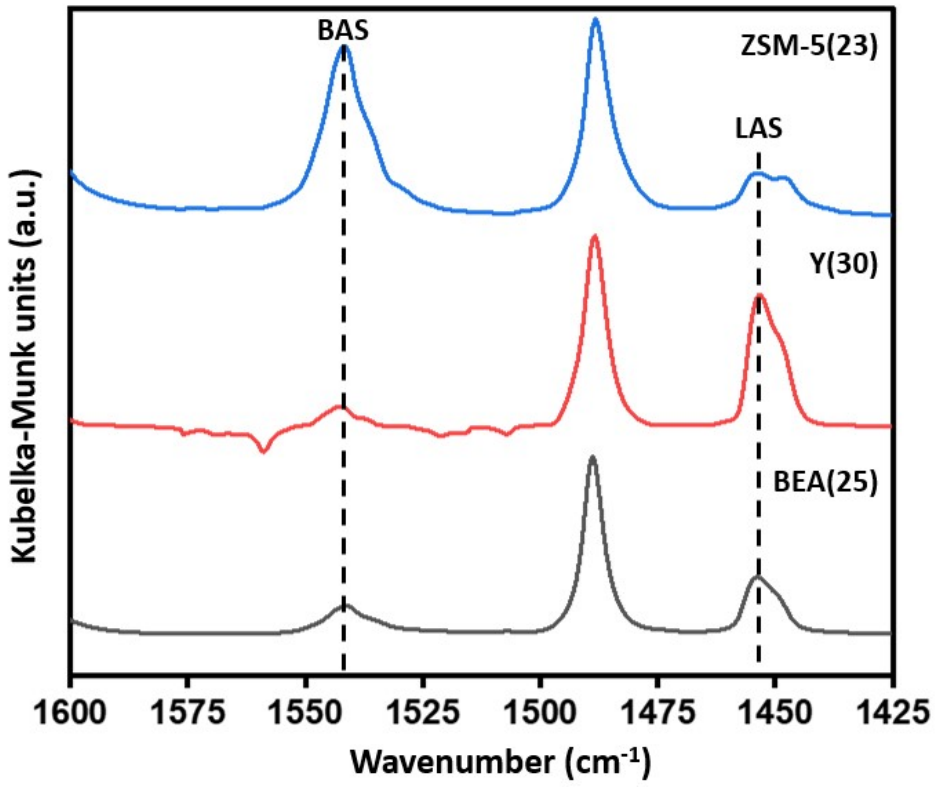

Fig. S11. Pyridine-IR spectra of BEA(25), Y(30) and ZSM-5(23).

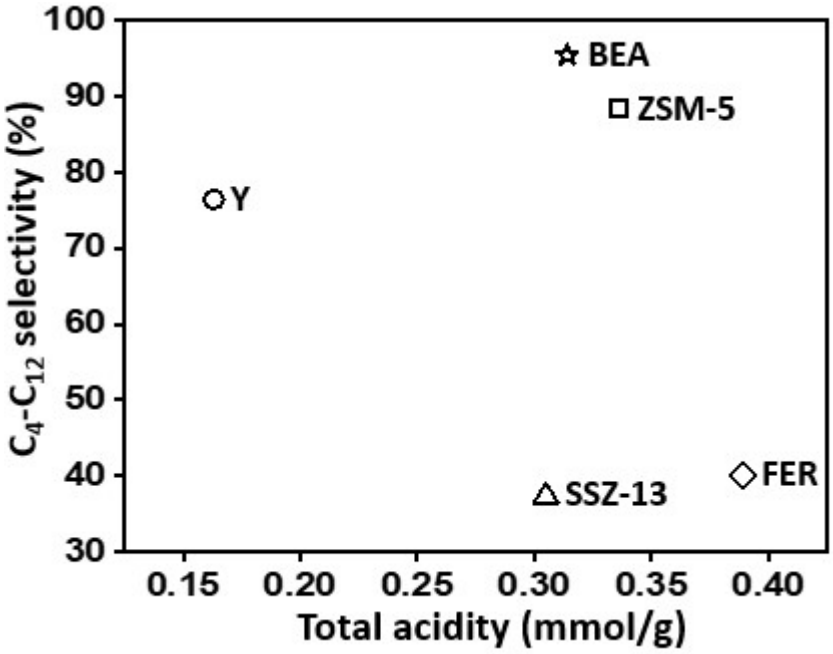

Fig. S12. Gasoline selectivity according to the total acidity of zeolites.

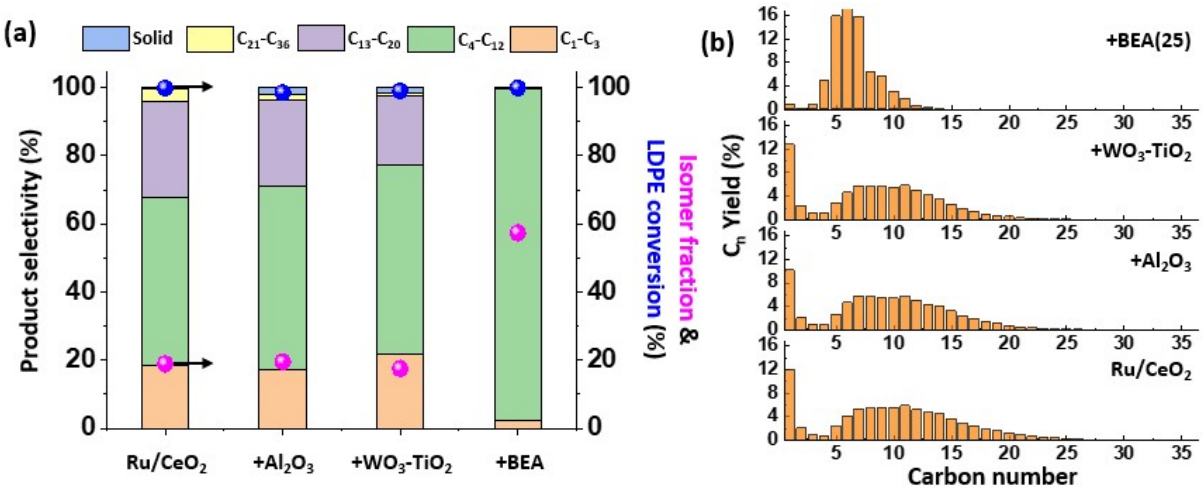

Fig. S13. (a) Product yield of LDPE hydroconversion and (b) product distribution over Ru/CeO_2 mixed with various acid catalysts. Reaction condition: 3.5 g LDPE, 0.125 g catalysts, 250 °C, 50 bar H_2, 16 h, mixing ratio of the Ru/CeO2 to acidic catalysts = 1:1.

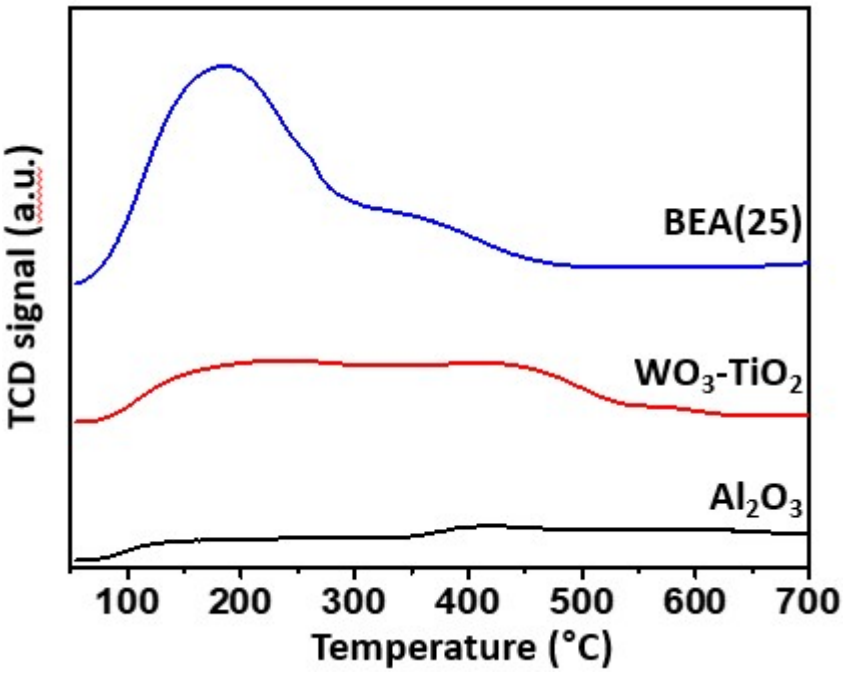

Fig. S14. NH_3-TPD of acidic catalysts.

	BET Surface area (m^2/g)[a]	Pore diameter (nm)[b]	Pore volume (cm^3/g)[c]	Total acidity (mmol/g)[d]
BEA(25)	**642**	**7.2**	**1.16**	**0.314**
Al_2O_3	**132**	**12.6**	**0.41**	**0.138**
WO_3-TiO_2	**171**	**6.6**	**0.28**	**0.174**

Table S6. Physicochemical properties of acid catalysts.

[a]Calculated by the BET equation.

[b]Average pore diameter.

[c]Total pore volume at $P/P_0 = 0.99$.

[d]Measured by NH_3-TPD.

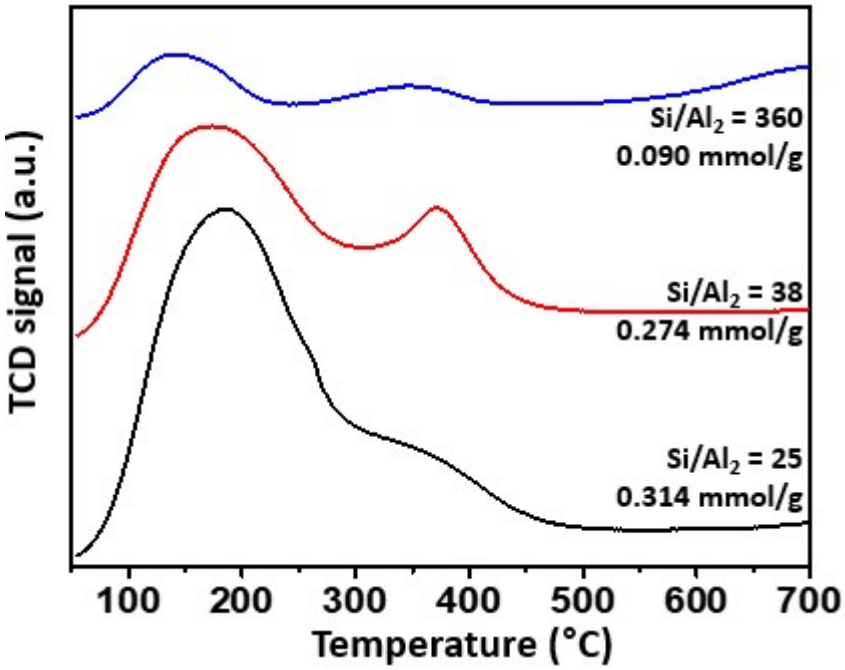

Fig. S15. NH_3-TPD of BEA zeolites with different acidity.

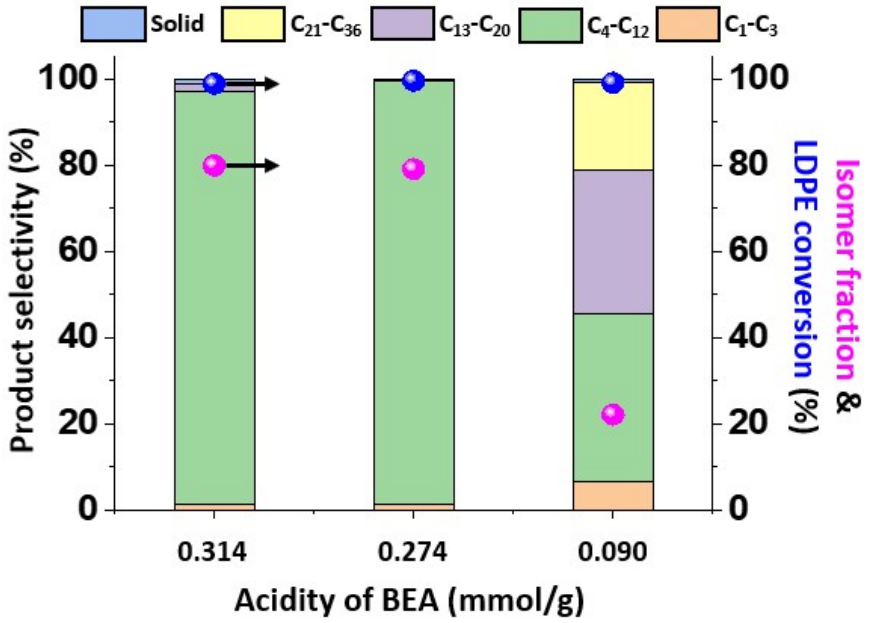

Fig. S16. Product yield of LDPE hydroconversion over the BEA with different acidity. Reaction condition: 3.5 g LDPE, 0.25 g catalysts, 260 °C, 50 bar H_2, 4 h, mixing ratio of the Ru/CeO_2 to BEA = 1:2.

Table S7. Physicochemical properties of Ru/CeO_2 and Ru/BEA.

	BET Surface area (m^2/g)[a]	Pore diameter (nm)[b]	Pore volume (cm^3/g)[c]	Ru dispersion (%)[d]	Ru particle size (nm)[d]	Total acidity (mmol/g)[e]
CeO_2	150	7.8	0.29	-	-	
$5Ru/CeO_2$	128	7.7	0.25	22.8	5.9	
BEA	642	7.2	1.16	-	-	0.314
5Ru/BEA	482	8.5	1.03	11.1	11.9	0.268

[a]Calculated by the BET equation.

[b]Average pore diameter.

[c]Total pore volume at $P/P_0 = 0.99$.

[d]Calculated by (cryo) pulse CO chemisorption.

[e]Measured by NH_3-TPD.

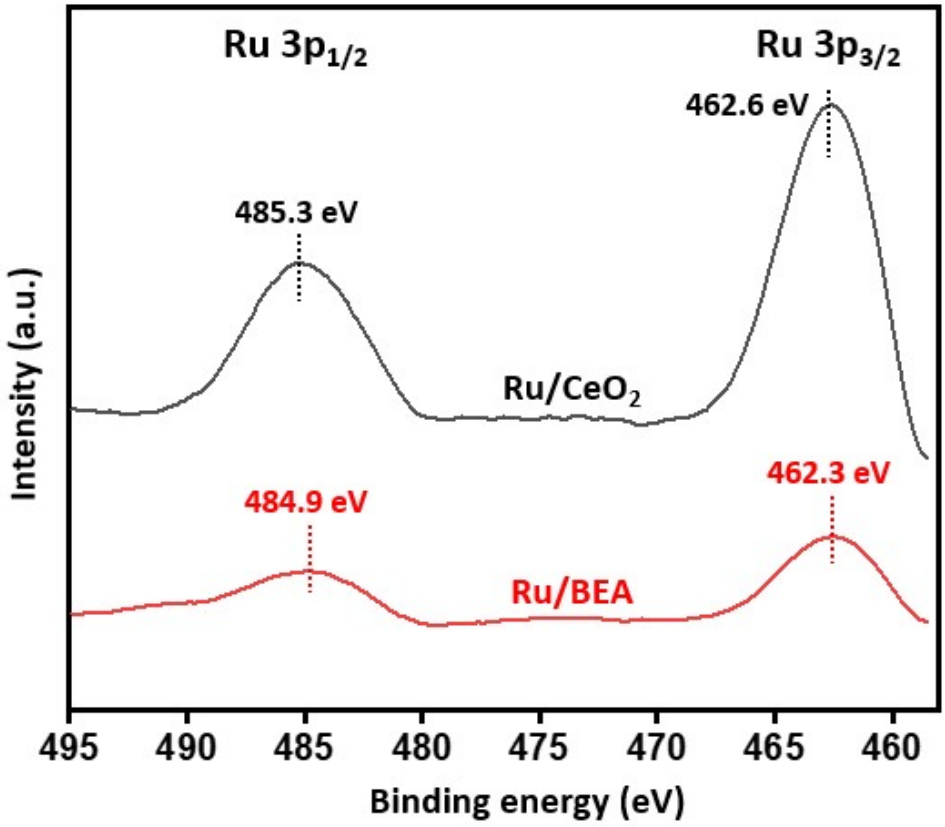

Fig. S17. XPS spectra of Ru/CeO_2 and Ru/BEA.

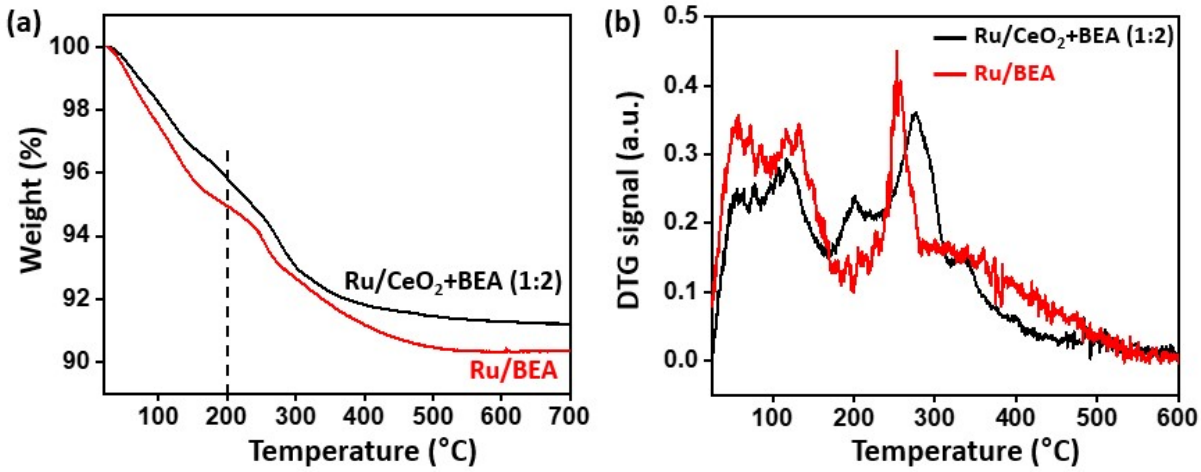

Fig. S18. (a) TGA and (b) DTG of post-reaction catalysts after octadecane (C_{18}) hydroconversion. Normalized TGA graph was obtained to take moisture and gaseous adsorbates into account.

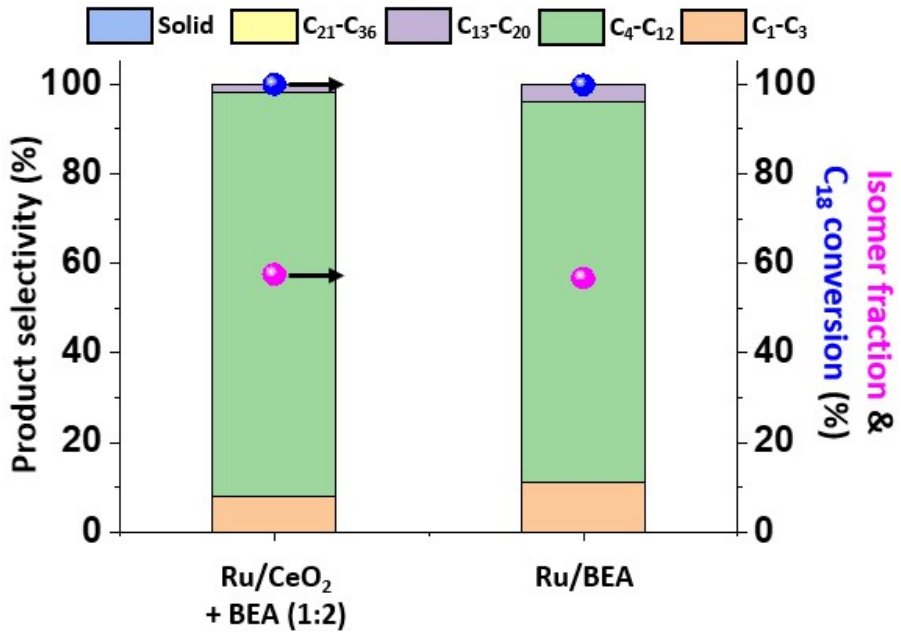

Fig. S19. Product yield of octadecane (C_{18}) hydroconversion over Ru/CeO_2+BEA and Ru/BEA. Model hydroconversion reaction using octadecane (C_{18}) was conducted to effectively separate the post-reaction catalysts from reactants and rule out the impact of unreacted PE. Reaction condition: 3.5 g C_{18}, 0.25 g for Ru/CeO_2+BEA and 0.0833g for Ru/BEA catalysts, 260 °C, 50 bar H_2, 3 h, mixing ratio of the Ru/CeO_2 to BEA = 1:2.

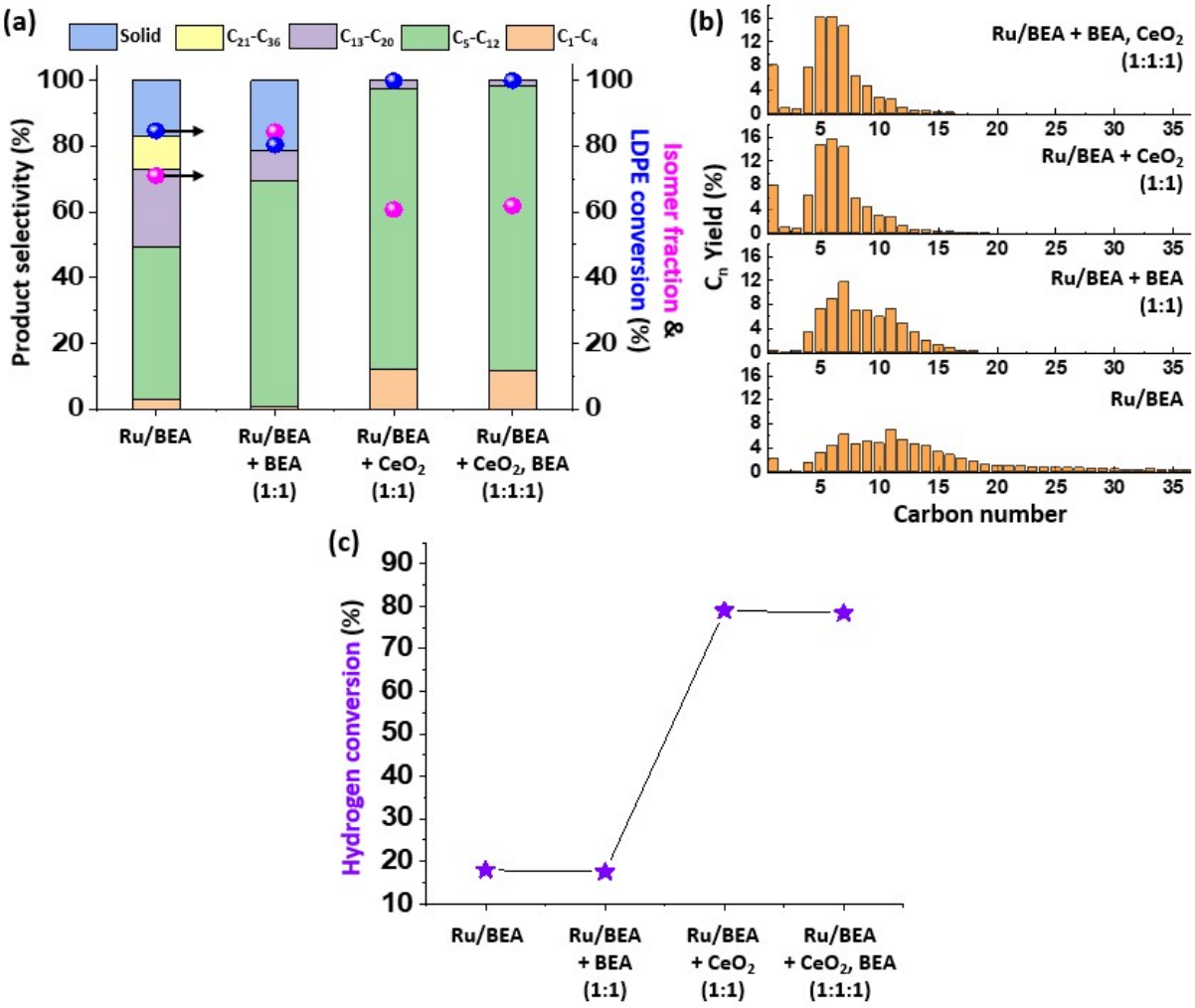

Fig. S20. (a) Product selectivity, LDPE conversion and isomer fraction in the gas and liquid products, (b) product distribution, and (c) hydrogen conversion over Ru/BEA and Ru/BEA mixture catalysts. Reaction condition: 3.5 g LDPE, 0.083 g for Ru/BEA, 0.1667 g for Ru/BEA+BEA (1:1) and Ru/BEA+CeO_2 (1:1) catalysts, and 0.25 g for Ru/BEA+CeO_2, BEA (1:1:1) catalyst (equal amount of Ru introduced), 260°C, 50 bar H_2, 4 h.

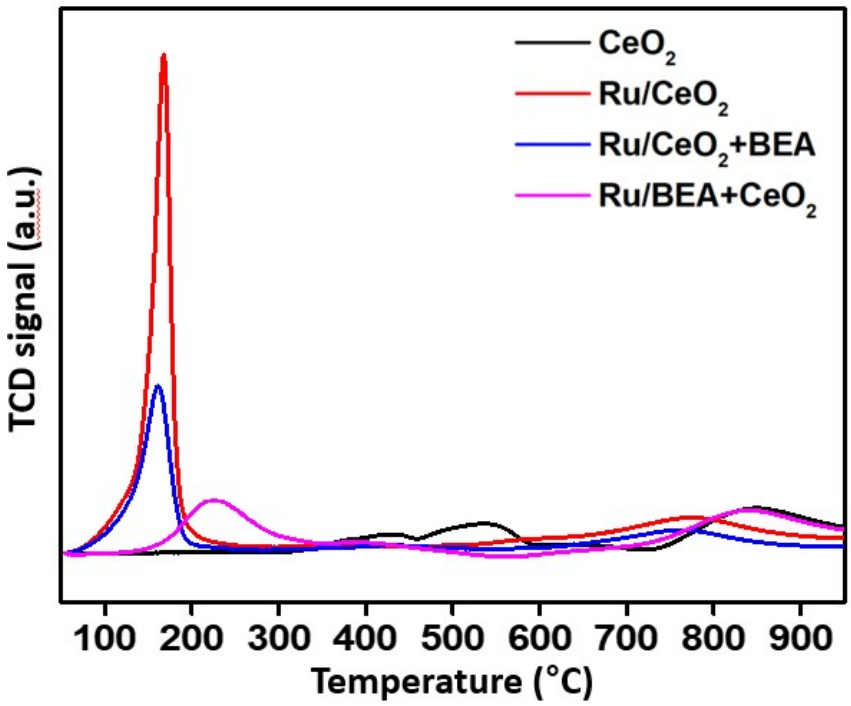

Fig. S21. H_2-TPR profiles of CeO_2, Ru/CeO_2, Ru/CeO_2+BEA (1:1), and Ru/BEA+CeO_2 (1:1) catalysts.

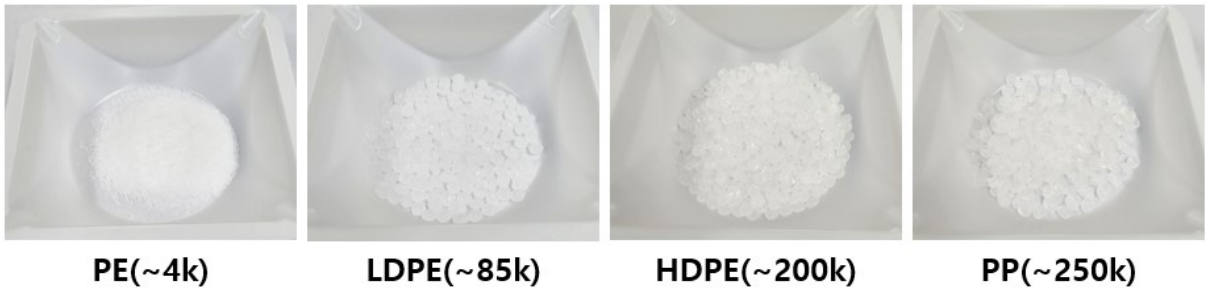

Fig. S22. Various PE and PP feeds obtained from Sigma-Aldrich.

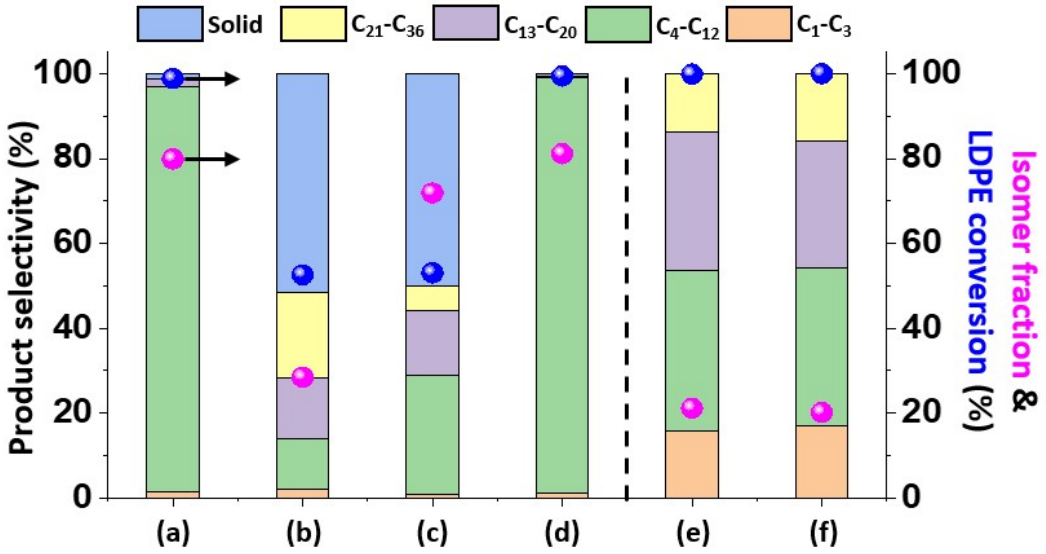

Fig. S23. Product selectivity, LDPE conversion and isomer fraction in the gas and liquid products. Reaction condition: 3.5 g LDPE, 0.25 g for Ru/BEA+CeO_2 catalysts, 260°C, 50 bar H_2, 4 h, (a) fresh catalyst; (b) post-reaction catalyst without regeneration; (c) post-reaction catalyst regenerated at 300°C for 3 h under static air and then 400°C for 3 h under 10% H_2/N_2 flow; (d) post-reaction catalyst without regeneration and adding 0.1667 g of fresh BEA; (e) fresh Ru/CeO_2; (f) post-reaction Ru/CeO_2 without regeneration.

References

1. Z. H. Wei, K. K. Zhu, L. Y. Xing, F. Yang, Y. S. Li, Y. R. Xu and X. D. Zhu, Rsc Adv, 2017, 7, 24015-24021.
2. Z. H. Wei, T. F. Xia, M. H. Liu, Q. S. Cao, Y. R. Xu, K. K. Zhu and X. D. Zhu, Front Chem Sci Eng, 2015, 9, 450-460.
3. Q. Du, X. Shang, Y. Y. Yuan, X. Su and Y. Q. Huang, Catalysts, 2025, 15.
4. L. X. Chen, L. C. Meyer, L. Kovarik, D. Meira, X. I. Pereira-Hernandez, H. H. Shi, K. Khivantsev, O. Y. Gutiérrez and J. Szanyi, Acs Catal, 2022, 12, 4618-4627.
5. M. Tamura, S. Miyaoka, Y. Nakaji, M. Tanji, S. Kumagai, Y. Nakagawa, T. Yoshioka and K. Tomishige, Applied Catalysis B-Environment and Energy, 2022, 318, 121870.
6. J. E. Rorrer, A. M. Ebrahim, Y. Questell-Santiago, J. Zhu, C. Troyano-Valls, A. S. Asundi, A. E. Brenner, S. R. Bare, C. J. Tassone, G. T. Beckham and Y. Roman-Leshkov, Acs Catal, 2022, 12, 13969-13979.
7. P. A. Kots, S. B. Liu, B. C. Vance, C. Wang, J. D. Sheehan and D. G. Vlachos, Acs Catal, 2021, 11, 8104-8115.
8. Y. Nakaji, M. Tamura, S. Miyaoka, S. Kumagai, M. Tanji, Y. Nakagawa, T. Yoshioka and K. Tomishige, Appl Catal B-Environ, 2021, 285, 119805.
9. W. T. Lee, A. van Muyden, F. D. Bobbink, M. D. Mensi, J. R. Carullo and P. J. Dyson, Nat Commun, 2022, 13, 4850.
10. C. Wang, T. J. Xie, P. A. Kots, B. C. Vance, K. W. Yu, P. Kumar, J. Y. Fu, S. B. Liu, G. Tsilomelekis, E. A. Stach, W. Q. Zheng and D. G. Vlachos, Jacs Au, 2021, 1, 1422-1434.
11. S. D. Jaydev, A. J. Martín, M. E. Usteri, K. Chikri, H. Eliasson, R. Erni and J. Pérez-Ramírez, Angew Chem Int Edit, 2024, 63.
12. Q. Y. Kang, M. Y. Chu, P. P. Xu, X. C. Wang, S. Q. Wang, M. H. Cao, O. Ivasenko, T. K. Sham, Q. Zhang, Q. M. Sun and J. X. Chen, Angew Chem Int Edit, 2023, 62.
13. J. C. Yan, G. N. Li, Z. W. Lei, X. L. Yuan, J. T. Li, X. R. Wang, B. Wang, F. P. Tian, T. Hu, L. Huang, Y. J. Ding, X. K. Xi, F. Zhu, S. Zhang, J. Li, Y. Chen, R. G. Cao and X. Wang, Nat Commun, 2025, 16, 2800.
14. S. B. Liu, P. A. Kots, B. C. Vance, A. Danielson and D. G. Vlachos, Sci Adv, 2021, 7, eabf8283.
15. A. Bin Jumah, V. Anbumuthu, A. A. Tedstone and A. A. Garforth, Ind Eng Chem Res, 2019, 58, 20601-20609.
16. X. Wu, A. Tennakoon, R. Yappert, M. Esveld, M. S. Ferrandon, R. A. Hackler, A. M. LaPointe, A. Heyden, M. Delferro, B. Peters, A. D. Sadow and W. Y. Huang, J Am Chem Soc, 2022, 144, 5323-5334.
17. M. Y. Sun, L. J. Zhu, W. Liu, X. P. Zhao, Y. F. Zhang, H. Luo, G. Miao, S. G. Li, S. Yin and L. Z. Kong, Sustain Energ Fuels, 2022, 6, 271-275.
18. X. T. Wu, X. Wang, L. L. Zhang, X. M. Wang, S. Y. Song and H. J. Zhang, Angew Chem Int Edit, 2024, 63.

19. L. Li, H. Luo, Z. L. Shao, H. Z. Zhou, J. W. Lu, J. J. Chen, C. J. Huang, S. A. Zhang, X. F. Liu, L. Xia, J. Li, H. Wang and Y. H. Sun, J Am Chem Soc, 2023, 145, 24433-24433.
20. B. W. Du, X. Chen, Y. Ling, T. T. Niu, W. X. Guan, J. P. Meng, H. Q. Hu, C. W. Tsang and C. H. Liang, Chemsuschem, 2023, 16.
21. J. Q. Cao, X. B. Gong, S. Li, Y. W. Wang, X. Feng, J. Gao and S. Shi, Chemcatchem, 2025, https://doi.org/10.1002/cctc.202501358.